ACS APPLIED MATERIALS & INTERFACES

Research Article

www.acsami.org

Edge Oxidation Effect of Chemical-Vapor-Deposition-Grown Graphene Nanoconstriction

Muhammad Waqas Iqbal,[†] Muhammad Zahir Iqbal,[†] Xiaozhan Jin,[‡] Chanyong Hwang,[‡] and Jonghwa Eom*,[†]

[†]Department of Physics and Graphene Research Institute, Sejong University, Seoul 143-747, Korea

[‡]Center for Nanometrology, Korea Research Institute of Standards and Science, Daejeon 305-340, Korea

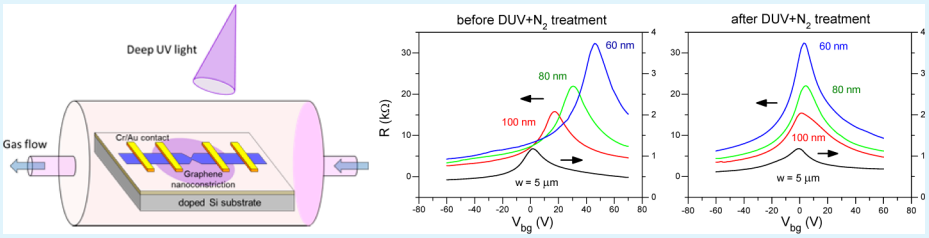

ABSTRACT: The edge oxidation effects of chemical-vapor-deposition-grown graphene devices with nanoconstrictions of different sizes are presented. The effects of edge oxidation on the doping level of a nanoconstriction graphene device were identified by Raman spectroscopy and using the back-gate-voltage-dependent resistance. Strong p-type doping was observed as the size of nanoconstriction decreased. The Dirac point of the graphene device shifted toward positive voltage, and the positions of the G and 2D peaks in Raman spectroscopy shifted toward a higher wave number, indicating the p-type doping effect of the graphene device. p-type doping was lifted by deep-ultraviolet light illumination under a nitrogen atmosphere at room temperature. p-type doping was restored by deep-ultraviolet light illumination under an oxygen atmosphere at room temperature. Edge oxidation in the narrow structures explains the origin of the p-type doping effect widely observed in graphene nanodevices.

KEYWORDS: *graphene, edge oxidation, nanoconstriction, doping, Raman spectroscopy, transport*

1. INTRODUCTION

Graphene, a two-dimensional planar layer of graphite, having weak spin−orbit coupling and ballistic conduction with chirality conservation, is a promising material for both fundamental investigations and potential applications owing to its exclusive electronic properties, especially its high carrier mobility at room temperature.[1,2] Electronic, optical, and mechanical properties make graphene a promising candidate material for applications such as sensors, ultrathin membranes, and transparent and flexible electrodes.[3] Recently, large-area graphene has been synthesized by chemical vapor deposition (CVD) using a copper or nickel catalyst. CVD-grown graphene can be easily transferred to an intended substrate using poly(methyl methacrylate) (PMMA) and poly(dimethylsiloxane) at comparatively low expense.[3−6]

The doping of graphene has received much attention owing to the critical need to fabricate integrated devices with convoluted structural design such as logic circuits. In recent times, there has been strong research interest in clusters and metal adatoms on graphene, for which it is known that there is local doping and modification of the band structure.[7,8] The band structure has also been modified when graphene is patterned at nanoscale. New phenomena found in graphene-based electronic devices have given rise to extensive theoretical studies.[9] Understanding the edge effects on the device performance is important because the modern nanolithography procedure is still far from achieving ideal atomistic precision.[10,11] The edges of lithography-patterned graphene nanoribbons are rough and have disordered regions. The charge density induced by functional groups of edges should vary from edge to center.[11,12] Consequently, it is essential to gain a better understanding of the unique properties of extremely narrow graphene devices, which are associated with the effects of edge chemistry and edge states in general. Covalent attachment of chemical groups and oxidation in particular can extensively modify the electronic properties of narrow graphene. To improve the transport properties of narrow graphene devices, it is critical to recognize the foremost sources of carrier scattering and functional groups on the edges.[11,13−15]

However, during standard fabrication processes employing oxygen plasma etching, an O_2 molecule mostly prefers to be adsorbed at the edge site among different chemisorption sites, where the edge trapping implies that the graphene edges become oxidized.[16−18] The effects of edge roughness and edge oxidation on the electronic structures and properties of nanopatterned graphene have already been reported on the theoretical stage.[9,14−18] Theories showed that the electronic

Received: December 20, 2013
Accepted: February 24, 2014
Published: February 24, 2014

   dx.doi.org/10.1021/am405885c | ACS Appl. Mater. Interfaces 2014, 6, 4207−4213

structure and transport properties of graphene nanoribbons are strongly affected by edge disorder and various functional groups present at edges. In fact, theories focused on graphene nanoribbons where the width is only a few nanometers. The edge effects of extremely narrow graphene devices remain experimentally unexplored.

In this paper, we show that the effect of edge oxidation increases with a decrease in the width of nanoconstriction. We have fabricated nanoconstriction devices of CVD-grown graphene and investigated the characteristics of devices by Raman spectroscopy and transport measurement. We found that the doping effect is locally dominant at the edges of graphene devices with nanoconstriction and that the doping can be controlled through deep-ultraviolet (DUV) light illumination with a gas flow.

2. EXPERIMENTAL SECTION

A graphene film was grown on 25-μm-thick copper foils from Alfa Aesar (99.8% pure) via thermal CVD. A mechanically polished and electropolished copper foil was inserted into a thermal CVD furnace. The furnace was evacuated to ~10^{-4} Torr, and the temperature rose to 1010 °C with H_2 gas flow (~10^{-2} Torr). After the temperature became stable at 1010 °C, both CH_4 [20 standard cubic centimeters per minute (sccm)] and H_2 (5 sccm) were injected into the furnace to synthesize the graphene for 8 min. After graphene synthesis, the sample was cooled at a rate of 50 °C/min to room temperature.[3,4]

Graphene films were transferred onto Si/SiO_2 wafers as follows. Copper foil was etched in an aqueous solution of ammonium persulfate. The surface of the graphene was spin-coated with PMMA, and the sample was then baked at 70 °C for 10 min. The PMMA coating was applied to prevent graphene films from cracking and folding during transfer to a desired substrate. PMMA/graphene film was washed with deionized water after the copper foil had been completely dissolved, and it was then transferred onto the Si/SiO_2 wafer. The PMMA film was removed with an organic solvent. The graphene sample was subsequently cleaned in isopropyl alcohol and dried in a N_2 gas flow.[3,4]

We fabricated graphene devices by employing photolithography, e-beam lithography, and oxygen plasma etching. Large electrode patterns with a chromium/gold (6/30 nm) film were deposited using a thermal evaporator after standard photolithography. E-beam lithography was then employed to pattern a direct ohmic contact on the graphene. Nanoconstrictions were produced by e-beam lithography and oxygen plasma etching; nanoconstrictions had different sizes of 60, 80, and 100 nm. The distance between contact electrodes is 5 μm, and the angle between graphene edges is 45° for all devices in this experiment. The width of the graphene ribbon is 5 μm for all nanoconstriction devices. A 5-μm-wide graphene strip was also fabricated as a reference device. The characteristics of a single-layer graphene were examined by optical microscopy and Raman spectroscopy.

Raman spectroscopy was carried out at the nanoconstriction of each graphene device. Raman mapping was also conducted to examine a CVD-grown graphene sheet at room temperature. The laser wavelength of the Raman microspectrometer was 514 nm, and the power was kept at less than l.0 mW to avoid a laser-induced heating effect. The laser spot size of Raman spectroscopy was 0.7 μm for a wavelength of 514 nm. The Dirac point of each graphene device was observed by gate-voltage-dependent resistance measurement using a four-probe measurement configuration with a lock-in amplifier. Electrical transport measurement was also performed for graphene nanoconstriction devices after exposure to DUV light with a wavelength of λ = 220 nm and an average intensity of 11 mW/cm^2 in N_2 gas flow for a certain time. The device was placed in a glass tube, and the glass tube was pumped to evacuate air. Then N_2 gas was introduced into the glass tube with continuous flow. DUV light was turned on to shine on the device in the glass tube. Figure 1a is a schematic diagram of the experimental setup of DUV light illumination.

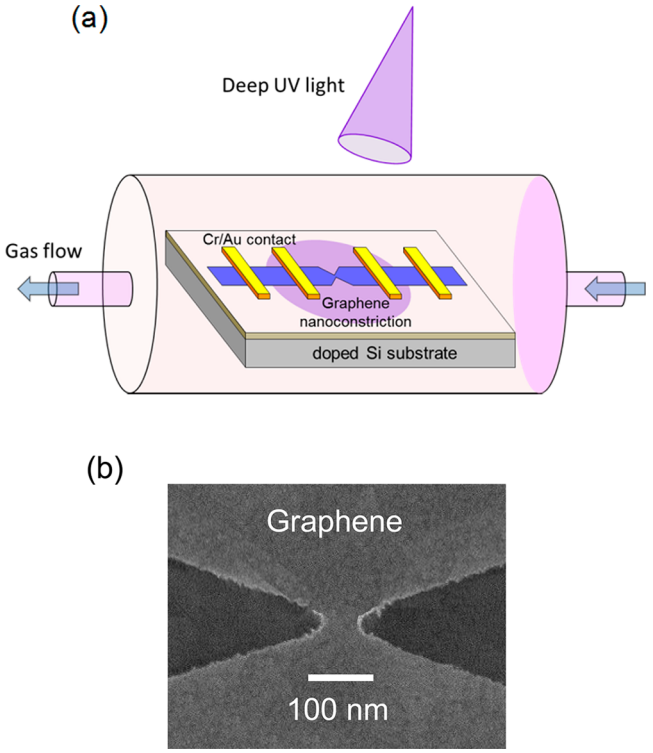

Figure 1. (a) Schematic diagram of DUV light illumination of a graphene device with a nanoconstriction with gas flow. (b) SEM image of a graphene device with a 60-nm-wide nanoconstriction.

Raman spectroscopy provides a convenient, nondestructive, and fast technique for characterizing the fundamental physical properties of various carbon materials, such as monolayer, bilayer, and stacked graphenes and single-walled/multiwalled carbon nanotubes.[19−21] Raman spectra of monolayer, bilayer, and multilayer graphene have two characteristic peaks (G and 2D). The G band is associated with the E_{2g} vibration mode of sp^2 bonds.[20−22] The 2D peak is the second order of the D peak and originates from a process where momentum conservation is satisfied by two phonons with opposite wave vectors.[21,22] The 2D peak is always present in Raman spectra of graphene. For single-layer graphene, the I_{2D}/I_G ratio must be greater than 2, and the full width at half-maximum (fwhm) of the 2D band is about 30 cm^{-1}. The D peak is due to A_{1g}-mode breathing vibrations of six-membered sp^2 carbon rings, which are absent in pure graphene.[21−24]

3. RESULTS AND DISCUSSION

Figure 1a is a schematic diagram of a graphene device with nanoconstriction and DUV light illumination with a gas flow. Figure 1b shows the scanning electron microscopy (SEM) image of a nanoconstriction device. As stated previously, the nanoconstriction widths (w) were 60, 80, and 100 nm, and a 5-μm-wide graphene device was examined as a reference sample.

Figure 2a shows the back-gate-voltage (V_{bg})-dependent resistance for the reference (5 μm) device and the CVD-grown graphene samples with different nanoconstriction widths. The maximum gate-dependent resistance identifies V_{bg} of the Dirac point, and the slope corresponds to the mobility of charge carriers in the graphene.[25−27] The Dirac point of the reference graphene (5-μm) sample was found to be around V_{bg} = 1.3 V, indicating an almost undoped characteristic of our sample. The Dirac points for 100-, 80-, and 60-nm-wide nanoconstrictions were observed at 16, 30, and 48 V, respectively. The Dirac points shifted toward more positive

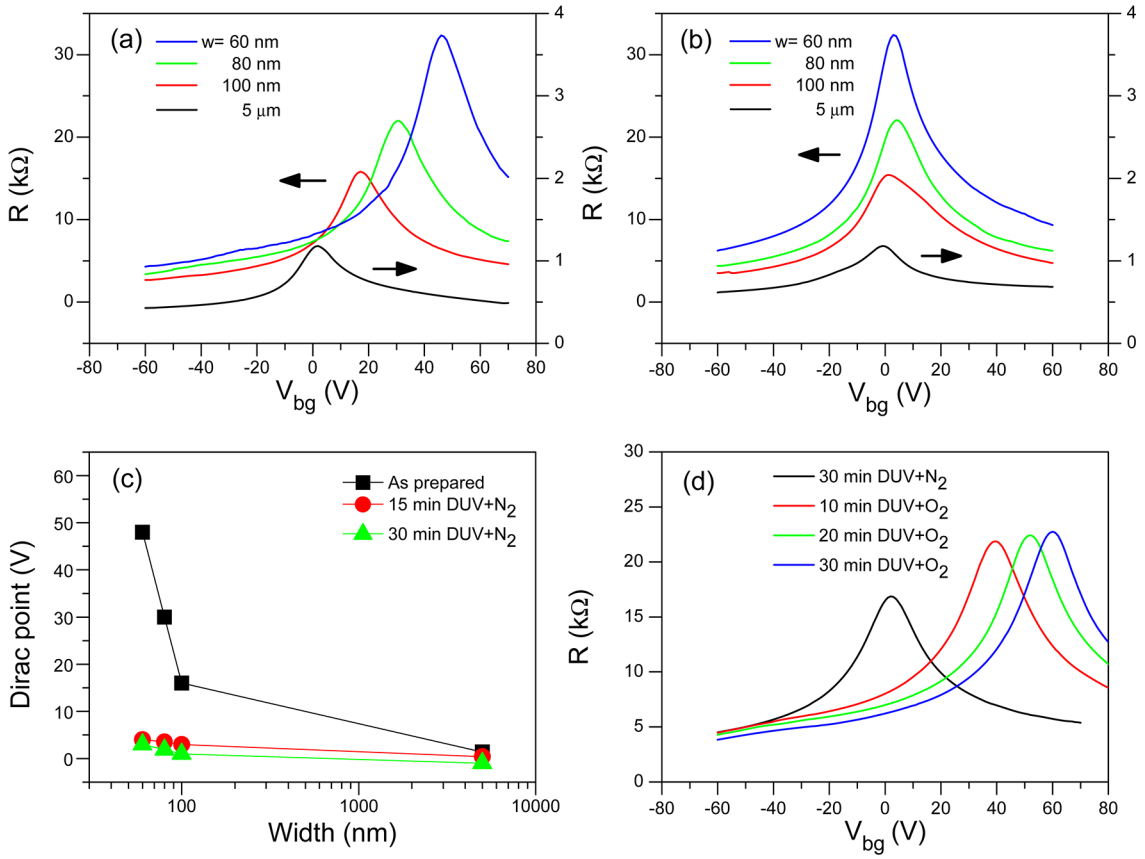

Figure 2. (a) V_{bg}-dependent resistance for the reference (w = 5 μm) and nanoconstrictions of CVD-grown graphene. Resistance is measured with four-probe geometry using standard lock-in amplifier techniques. The Dirac point of the reference graphene sample is around V_{bg} = 1.3 V, indicating an almost undoped characteristic of pristine graphene. The arrows indicate the y-axis scale for reference and different nanoconstriction graphene samples. The rightward arrow indicates the scale for the reference sample, whereas the leftward arrow indicates the scale for nanoconstriction devices. (b) V_{bg}-dependent resistance of the reference and nanoconstriction samples after 30 min of DUV illumination with a N_2 gas flow. DUV+N_2 treatment results in the shift of the Dirac point toward V_{bg} = 0 V. (c) Dirac point as a function of the nanoconstriction width for the as-prepared graphene and after different DUV+N_2 exposure times. (d) Experiment started with the device having a 100-nm-wide nanoconstriction after 30 min of DUV+N_2 treatment. DUV+O_2 treatment was applied to restore the p-type doping of nanoconstriction. V_{bg}-dependent resistance after 10, 20, and 30 min of DUV exposure in an oxygen atmosphere. The Dirac points were observed at V_{bg} = 39, 52, and 60 V after 10, 20, and 30 min of DUV+O_2 treatment, respectively.

gate voltages as the width of nanoconstriction decreased, indicating the p-type doping of the graphene. As the nanoconstriction width decreased, the resistance of a graphene device increased, and a stronger p-type doping effect was observed.

Asymmetry is found in the V_{bg}-dependent resistivity of the graphene devices (see Figure 2a). Because the band structures of graphene for the hole and electron are symmetric, the mobilities of the electron and hole are expected to be equal. Therefore, one can expect a symmetric V_{bg}-dependent resistivity with respect to the Dirac point. However, in normal graphene devices, the hole mobility is higher than the electron mobility because of the different scattering cross sections for the electron and hole by charge impurity in the relativistic dispersion.[28] Because the slope of the conductivity, $d\sigma/dV_g$, is proportional to mobility, the asymmetry in the V_{bg}-dependent resistivity has been consistently observed in graphene devices in this paper.

Figure 2b shows the gate-dependent resistances of the graphene devices after 30 min of DUV exposure in a N_2 gas flow (DUV+N_2). DUV+N_2 exposure of the graphene device shifted the Dirac point toward 0 V. The shift in the Dirac point due to DUV+N_2 treatment is shown in Figure 2c. The Dirac points of the reference graphene device and devices with 100-, 80-, and 60-nm-wide nanoconstrictions were observed at 1.3, 16, 31, and 47 V, respectively, for the as-prepared condition (before DUV+N_2 treatment). After 15 min of DUV+N_2 exposure of the graphene devices, the Dirac points shifted to 0.4, 3, 3.5, and 4 V, respectively. The Dirac points shifted further to 0, 1.1, 1.9, and 3 V, respectively, after 30 min of DUV +N_2 exposure. We found that exposure to DUV affects the Dirac point and that the position of the Dirac point remains almost the same for a N_2 gas flow without DUV illumination. DUV illumination should provide the energy required for the reaction of nitrogen atoms with oxygen atoms, which were originally adhered to graphene. A minimum amount of energy is required to release oxygen from the surface of graphene.[29−31]

Figure 2d shows the gate-voltage-dependent resistance for the graphene device with a 100-nm-wide nanoconstriction after 10, 20, and 30 min of DUV exposure in an O_2 gas flow (DUV +O_2). The Dirac points were observed at 39, 52, and 60 V after 10, 20, and 30 min of DUV+O_2 treatment, respectively. Oxygen adsorption on graphene should have a p-type doping effect. The adsorption of oxygen on a graphene film has already been studied.[32−34] However, we found that the effect of oxygen doping is more significant when graphene is exposed to DUV

dx.doi.org/10.1021/am405885c | ACS Appl. Mater. Interfaces 2014, 6, 4207−4213

light. DUV light provides enough energy for electrons to adsorb onto, or desorb from, the surface of graphene.

Raman spectra of the nanoconstrictions and reference graphene are shown in Figure 3a. The Raman spectra indicate the overall behavior of a single-layer graphene. The D peak became more pronounced as the width of nanoconstriction decreased. G and 2D peaks were observed at 1581 and 2682 cm^{-1}, respectively, for the reference graphene device. As an indication that the samples were single-layer graphene structures, we found that the intensity of the 2D peak was 3 times that of the G peak and the fwhm of the 2D band of the reference graphene was about 30 cm^{-1}. The absence of the D peak in the reference graphene indicates the high quality of the reference. However, the D peak appeared for nanoconstriction devices, and the D-band intensity increased drastically as the width of nanoconstriction decreased. The observation of the D peak was accompanied by a pronounced D′ peak at 1624 cm^{-1} and a D + D′ peak around 2945 cm^{-1}. We note that D′ and D + D′ peaks were not observed for the reference graphene but became prominent for nanoconstrictions.

Figure 3b shows the shift in the positions and change in the intensities of the G and 2D peaks. While the G band was observed at 1581 cm^{-1} for the reference graphene, it was found at 1585, 1591, and 1597 cm^{-1} for nanoconstriction widths of 100, 80, and 60 nm, respectively. There was a blue shift of 16 cm^{-1} in the G band for 60-nm-wide nanoconstriction relative to the reference graphene. There was also a blue shift in the 2D band for nanoconstrictions. While the 2D band of the reference graphene was observed at 2682.1 cm^{-1}, those of nanoconstrictions with widths of 100, 80, and 60 nm were observed at 2686.3, 2694.2, and 2699.1 cm^{-1}, respectively. There was a blue shift of 17 cm^{-1} in the peak position of the 2D band for 60-nm-wide nanoconstriction relative to the reference graphene. Figure 3c shows Lorentzian fits for the G and D′ peaks. Red circles represent the experimental data, and black, blue, and green lines are the Lorentzian fits for the G, D′, and combined peaks, respectively. The fwhm's of the G band were 16, 14, 13.1, and 11.5 cm^{-1} for the reference and nanoconstriction widths of 100, 80, and 60 nm, respectively. The blue shifts of the G and 2D band positions are known to be associated with p-type doping of graphene, and doping reduces the fwhm of the G peak.[35]

The blue shift of the G and 2D peaks and reduction of the fwhm of the G peak indicate a p-type doping effect, which can be also confirmed by the electrical measurement of the graphene device.[35−41] Our experimental observations clearly indicate the p-type doping of the graphene device when patterned with nanoconstriction. The doping effect is closely related to the adsorption of O_2 molecules at the edge of nanoconstriction during the patterning process. During the patterning process, the entire area is covered with PMMA so that O_2 molecules can attach mostly to the graphene pattern edges. Here O_2 trapping implies that the graphene edges become oxidized and p-type-doped.[10,11,17,18]

The width of the graphene ribbon is kept the same as 5 μm for all devices in the experiment. Therefore, the effect of the distance between edges on edge oxidation can be seen by changing the width of nanoconstriction. As we reduce the nanoconstriction width, electrons passing through narrower nanoconstriction are more actively affected by oxidized edges. Actually, Figure 2a shows the effect of the distance between edges on edge oxidation. Figure 2c shows that effect of the distance between edges on an edge−edge-redox reaction. When the distance between edges decreases in nanoconstriction, the influence by the edge oxidation (or edge-redox reaction) on the transport properties becomes more dominant.

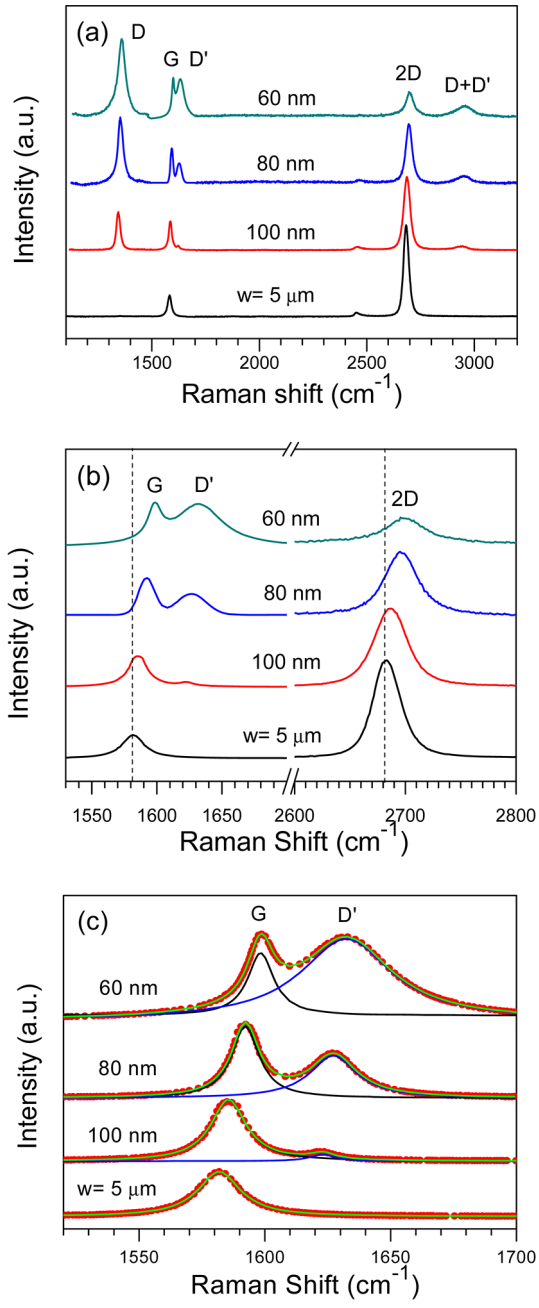

Figure 3. (a) Raman spectra of the as-prepared reference and nanoconstriction devices. (b) Shifts in the positions of the G and 2D peaks. G-band peaks in Raman spectra were observed at 1582.1, 1585.3, 1591.2, and 1598.1 cm^{-1} for the reference (w = 5 μm) and nanoconstrictions (w = 100, 80, and 60 nm), respectively. 2D-band peaks in Raman spectra were observed at 2682.1, 2686.3, 2694.2, and 2699.1 cm^{-1} for the reference (w = 5 μm) and nanoconstrictions (w = 100, 80, and 60 nm), respectively. (c) Lorentzian fits for the reference (w = 5 μm) and nanoconstrictions (w = 100, 80, and 60 nm). Red circles represent the experimental data, and black, blue, and green lines are the Lorentzian fits for the G, D′, and combined peaks, respectively. fwhm's of the G-band peaks are 16, 14, 13.1, and 11.5 cm^{-1} for the reference (w = 5 μm) and nanoconstrictions (w = 100, 80, and 60 nm), respectively.

dx.doi.org/10.1021/am405885c | ACS Appl. Mater. Interfaces 2014, 6, 4207−4213

We performed an experiment to remove oxygen at the edge of nanoconstriction and checked the effect of the redox reaction. Oxygen at the edge was removed by DUV illumination with a N_2 gas flow (DUV+N_2) for 15 min. Figure 4a shows Raman spectra of the reference graphene (w = 5 μm) and nanoconstrictions after DUV+N_2 treatment. There were

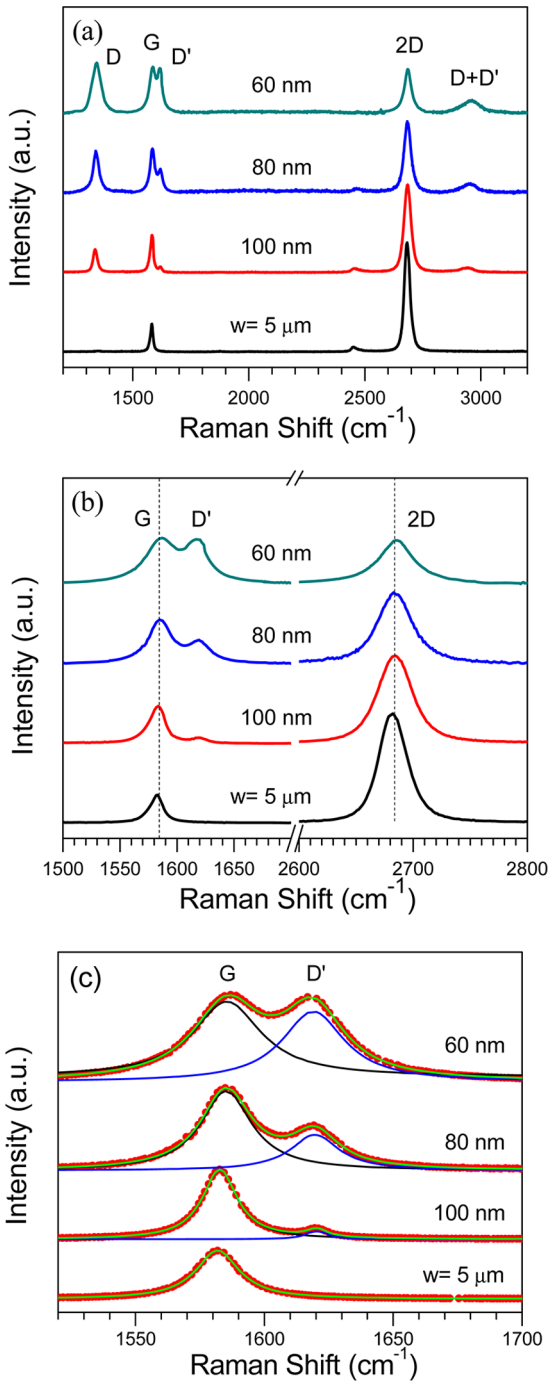

Figure 4. (a) Raman spectra of the reference and nanoconstriction graphene devices after 15 min of DUV+N_2 treatment. (b) Enlarged Raman spectra for the peak positions of the G and 2D bands after 15 min of DUV+N_2 treatment. (c) Lorentzian fits for the reference (w = 5 μm) and nanoconstrictions (w = 100, 80, and 60 nm) after 15 min of DUV+N_2 treatment. Red circles represent the experimental data, and black, blue, and green lines are the Lorentzian fits for the G, D′, and combined peaks, respectively.

significant changes in the Raman spectra. First, the intensity of the D peak decreased with DUV+N_2 treatment. The decrease in the D peak intensity should be due to removal of the oxygen functional groups from the edges. Second, the positions of the G and 2D peaks of nanoconstrictions after DUV+N_2 treatment were the same as those of the reference graphene, as shown in Figure 4b. The main features of Raman spectra indicate that p-type doping was lifted by 15 min of DUV+N_2 treatment. Figure 4c shows Lorentzian fits for the G and D′ peaks of nanoconstrictions after 15 min of DUV+N_2 treatment. Red circles represent the experimental data, and black, blue, and green lines are the Lorentzian fits for the G, D′, and combined peaks, respectively. We note that the fwhm of the G peak for nanoconstriction after DUV+N_2 treatment was greater than that of the G peaks in Figure 3c. The p-type doping of nanoconstriction was restored if DUV+O_2 treatment was applied to the sample, as shown in Figure 2d.

We examined the location of oxygen adsorption on the graphene devices with nanoconstrictions. Figure 5a shows the

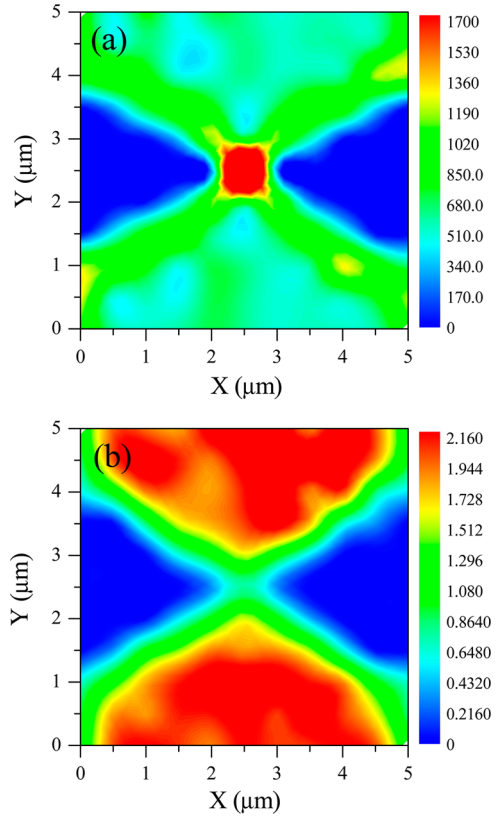

Figure 5. (a) Raman mapping of the intensity of the D peak for the graphene device with 60-nm-wide nanoconstriction. (b) Raman mapping of the peak intensity ratio I_{2D}/I_G for the graphene device with 60-nm-wide nanoconstriction. The minimum I_{2D}/I_G was observed in the area of nanoconstriction.

Raman D-peak intensity mapping of 60-nm-wide nanoconstriction. The intensity is scaled by color from blue to red. While the D-peak intensity was low in the wide graphene area, the highest D-peak intensity was found at nanoconstriction. However, the D-peak intensity was high at edges of the graphene, which is related to the edge roughness and the presence of oxygen and different functional groups on the edges. Figure 5b shows the Raman mapping of the I_{2D}/I_G ratio for 60-nm-wide nanoconstriction. The minimum magnitude of

dx.doi.org/10.1021/am405885c | ACS Appl. Mater. Interfaces 2014, 6, 4207−4213

I_{2D}/I_G was observed at nanoconstriction. The magnitude of I_{2D}/I_G was also low at the graphene edges. In the middle of the graphene away from the edges, the I_{2D}/I_G ratio was higher. We can confirm that oxygen adsorption was dominant at nanoconstriction. To confirm further the occurrence of oxygen adsorption, the nanoconstriction device was examined by energy-dispersive X-ray spectroscopy. The oxygen adsorption at nanoconstriction should be effectively removed by DUV+N_2 treatment to lift the p-type doping effect. Table 1 presents the results of analysis by energy-dispersive X-ray spectroscopy before and after DUV+N_2 treatment for three devices with 60-nm-wide nanoconstriction. The X-rays were scanned on an area of 120 × 120 nm^2 centered on nanoconstriction to get the average value of the atomic elements. The relative amount of oxygen at nanoconstriction decreased by the amount of ~2.5% after DUV+N_2 treatment. The background signal for oxygen, mostly originating from a 300-nm-thick SiO_2 capping layer, is large, and hence the change of oxygen looks small. However, a ~2.5 % reduction of the amount of oxygen was consistently observed after DUV+N_2 treatment for all devices, as shown in Table 1.

Table 1. Energy-Dispersive X-ray Spectroscopy Results for the Graphene Device with 60-nm-Wide Nanoconstriction before and after DUV+N_2 Treatment[a]

Device No.	Element	Before DUV+N_2 treatment	After DUV+N_2 treatment
1	C	2.10% ± 0.004%	2.10% ± 0.003%
	O	24.57% ± 0.005%	22.12% ± 0.002%
2	C	2.14% ± 0.003%	2.14% ± 0.002%
	O	24.60% ± 0.004%	22.14% ± 0.005%
3	C	2.09% ± 0.003%	2.09% ± 0.004%
	O	24.55% ± 0.005%	22.11% ± 0.003%

[a]X-rays were focused on the area of nanoconstriction. The relative amount of oxygen at nanoconstriction decreased from 24.57% to 22.12% with DUV+N_2 treatment.

4. CONCLUSION

We fabricated graphene devices with nanoconstrictions and examined the characteristics of the devices through Raman spectroscopy and transport measurements. Raman spectra and transport measurements indicated that nanoconstriction affects the structural confinement and electronic properties of the CVD-grown graphene. The blue shift in the G and 2D Raman peak positions indicated p-type doping in the graphene nanoconstriction devices. However, red shifts in the G and 2D peak positions with DUV+N_2 exposure indicated the dedoping of nanoconstrictions. The doping effect is attributed to the adsorption of O_2 molecules at nanoconstriction and edges of the graphene during the patterning process. As the width of nanoconstriction decreases, the effect of the edge oxidation state becomes more dominant in electronic transport. Oxygen atoms are bound to the carbon atom present at nanoconstriction. Oxygen atoms can be desorbed by DUV illumination with a N_2 gas flow. Oxygen atoms are likely to form NO molecules in a N_2-gas environment, and NO molecules are then desorbed from graphene with the aid of DUV illumination.

Raman mapping of the D peak and I_{2D}/I_G shows that the adsorption site is located at nanoconstriction. Energy-dispersive X-ray spectroscopy of nanoconstriction further confirms that oxygen is the element for p-type doping and that DUV+N_2 treatment effectively removes oxygen atoms at nanoconstriction, leading to a dedoping effect. p-type doping is restored by applying DUV light illumination under an oxygen atmosphere at room temperature. The edge oxidation of narrow structures explains the origin of the p-type doping effect widely observed in graphene nanodevices.

AUTHOR INFORMATION

Corresponding Author

*E mail: eom@sejong.ac.kr. Tel: +82-2-3408-3794.

Notes

The authors declare no competing financial interest.

ACKNOWLEDGMENTS

This research was supported by the Nano-Material Technology Development Program (Grant 2012M3A7B4049888) and the Converging Research Center Program (Grant 2013K000172) through the National Research Foundation of Korea (NRF) funded by the Ministry of Science, ICT, and Future Planning. This research was also supported by the Basic Science Research Program (Grants 2010-0020207 and 2013R1A1A2061396) through the NRF funded by the Ministry of Education.

REFERENCES

(1) Geim, A. K.; Novoselov, K. S. The rise of graphene. *Nat. Mater.* **2007**, *6*, 183−191.
(2) Castro Neto, A. H.; Guinea, F.; Peres, N. M. R.; Novoselov, K. S.; Geim, A. K. The electronic properties of graphene. *Rev. Mod. Phys.* **2009**, *81*, 109−162.
(3) Kim, K. S.; Zhao, Y.; Jang, H.; Lee, S. Y.; Kim, J. M.; Kim, K. S.; Ahn, J. H.; Kim, P.; Choi, J. Y.; Hong, B. H. Large-scale pattern growth of graphene films for stretchable transparent electrodes. *Nature* **2009**, *457*, 706−710.
(4) Li, X. S.; Zhu, Y. W.; Cai, W. W.; Borysiak, M.; Han, B. Y.; Chen, D.; Piner, R. D.; Colombo, L.; Ruoff, R. S. Transfer of Large-Area Graphene Films for High-Performance Transparent Conductive Electrodes. *Nano Lett.* **2009**, *9*, 4359−4363.
(5) Lee, Y.; Bae, S.; Jang, H.; Jang, S.; Zhu, S. E.; Sim, S. H.; Song, Y. I.; Hong, B. H.; Ahn, J. H. Wafer-Scale Synthesis and Transfer of Graphene Films. *Nano Lett.* **2010**, *10*, 490−493.
(6) Lin, Y. C.; Jin, C. H.; Lee, J. C.; Jen, S. F.; Suenaga, K.; Chiu, P. W. Clean Transfer of Graphene for Isolation and Suspension. *ACS Nano* **2011**, *5*, 2362−2368.
(7) Katsnelson, M. I.; Guinea, F.; Geim, A. K. Scattering of electrons in graphene by clusters of impurities. *Phys. Rev. B* **2009**, *79*, 195426.
(8) Uchoa, B.; Kotov, V. N.; Peres, N. M. R.; Neto, A. H. C. Localized magnetic states in graphene. *Phys. Rev. Lett.* **2008**, *101*, 026805.
(9) Yoon, Y.; Guo, J. Effect of edge roughness in graphene nanoribbon transistors. *Appl. Phys. Lett.* **2007**, *91*, 073103.
(10) Chitara, B.; Panchakarla, L. S.; Krupanidhi, S. B.; Rao, C. N. R. Infrared Photodetectors Based on Reduced Graphene Oxide and Graphene Nanoribbons. *Adv. Mater.* **2011**, *23*, 5419−5424.
(11) Biro, L. P.; Lambin, P. Nanopatterning of graphene with crystallographic orientation control. *Carbon* **2010**, *48*, 2677−2689.
(12) Sinitskii, A.; Tour, J. M. Patterning graphene nanoribbons using copper oxide nanowires. *Appl. Phys. Lett.* **2012**, *100*, 103106.
(13) Fang, T.; Konar, A.; Xing, H.; Jena, D. Mobility in semiconducting graphene nanoribbons: Phonon, impurity, and edge roughness scattering. *Phys. Rev. B* **2008**, *78*, 205403.
(14) Goharrizi, A. Y.; Pourfath, M.; Fathipour, M.; Kosina, H.; Selberherr, S. An Analytical Model for Line-Edge Roughness Limited Mobility of Graphene Nanoribbons. *IEEE Trans. Electron Dev.* **2011**, *58*, 3725−3735.

(15) Yazdanpanah, A.; Pourfath, M.; Fathipour, M.; Kosina, H.; Selberherr, S. A Numerical Study of Line-Edge Roughness Scattering in Graphene Nanoribbons. *IEEE Trans. Electron Dev.* **2012**, *59*, 433−440.
(16) Hod, O.; Barone, V.; Peralta, J. E.; Scuseria, G. E. Enhanced half-metallicity in edge-oxidized zigzag graphene nanoribbons. *Nano Lett.* **2007**, *7*, 2295−2299.
(17) Lee, G.; Cho, K. Electronic structures of zigzag graphene nanoribbons with edge hydrogenation and oxidation. *Phys. Rev. B* **2009**, *79*, 165440.
(18) Yu, S. S.; Zheng, W. T.; Jiang, Q. Oxidation of Graphene Nanoribbon by Molecular Oxygen. *IEEE Trans. Nanotechnol.* **2008**, *7*, 628−635.
(19) Dresselhaus, M. S.; Jorio, A.; Hofmann, M.; Dresselhaus, G.; Saito, R. Perspectives on Carbon Nanotubes and Graphene Raman Spectroscopy. *Nano Lett.* **2010**, *10*, 751−758.
(20) Ferrari, A. C. Raman spectroscopy of graphene and graphite: Disorder, electron−phonon coupling, doping and nonadiabatic effects. *Solid State Commun.* **2007**, *143*, 47−57.
(21) Dresselhaus, M. S.; Dresselhaus, G.; Saito, R.; Jorio, A. Raman spectroscopy of carbon nanotubes. *Phys. Rep.* **2005**, *409*, 47−99.
(22) Niyogi, S.; Bekyarova, E.; Itkis, M. E.; Zhang, H.; Shepperd, K.; Hicks, J.; Sprinkle, M.; Berger, C.; Lau, C. N.; Deheer, W. A. Spectroscopy of covalently functionalized graphene. *Nano Lett.* **2010**, *10*, 4061−4066.
(23) Ferrari, A. C.; Meyer, J. C.; Scardaci, V.; Casiraghi, C.; Lazzeri, M.; Mauri, F.; Piscanec, S.; Jiang, D.; Novoselov, K. S.; Roth, S.; Geim, A. K. Raman spectrum of graphene and graphene layers. *Phys. Rev. Lett.* **2006**, *97*, 187401.
(24) Kalbac, M.; Reina-Cecco, A.; Farhat, H.; Kong, J.; Kavan, L.; Dresselhaus, M. S. The Influence of Strong Electron and Hole Doping on the Raman Intensity of Chemical Vapor-Deposition Graphene. *ACS Nano* **2010**, *4*, 6055−6063.
(25) Tan, Y. W.; Zhang, Y.; Bolotin, K.; Zhao, Y.; Adam, S.; Hwang, E. H.; Das Sarma, S.; Stormer, H. L.; Kim, P. Measurement of scattering rate and minimum conductivity in graphene. *Phys. Rev. Lett.* **2007**, *99*, 246803.
(26) Morozov, S. V.; Novoselov, K. S.; Katsnelson, M. I.; Schedin, F.; Elias, D. C.; Jaszczak, J. A.; Geim, A. K. Giant intrinsic carrier mobilities in graphene and its bilayer. *Phys. Rev. Lett.* **2008**, *100*, 016602.
(27) Chen, J. H.; Jang, C.; Adam, S.; Fuhrer, M. S.; Williams, E. D.; Ishigami, M. Charged-impurity scattering in graphene. *Nat. Phys.* **2008**, *4*, 377−381.
(28) Novikov, D. Numbers of donors and acceptors from transport measurements in graphene. *Appl. Phys. Lett.* **2007**, *91*, 102102.
(29) Dai, J. Y.; Yuan, J. M. Modulating the electronic and magnetic structures of P-doped graphene by molecule doping. *J. Phys.: Condens. Matter* **2010**, *22*, 225501.
(30) Chen, Y.; Gao, B.; Zhao, J. X.; Cai, Q. H.; Fu, H. G. Si-doped graphene: an ideal sensor for NO- or NO2-detection and metal-free catalyst for N_2O-reduction. *J. Mol. Model.* **2012**, *18*, 2043−2054.
(31) Nourbakhsh, A.; Cantoro, M.; Klekachev, A. V.; Pourtois, G.; Vosch, T.; Hofkens, J.; van der Veen, M. H.; Heyns, M. M.; De Gendt, S.; Sels, B. F. Single Layer vs Bilayer Graphene: A Comparative Study of the Effects of Oxygen Plasma Treatment on Their Electronic and Optical Properties. *J. Phys. Chem. C* **2011**, *115*, 16619−16624.
(32) Batzill, M. The surface science of graphene: Metal interfaces, CVD synthesis, nanoribbons, chemical modifications, and defects. *Surf. Sci. Rep.* **2012**, *67*, 83−115.
(33) Yu, L.; Pan, X. L.; Cao, X. M.; Hu, P.; Bao, X. H. Oxygen reduction reaction mechanism on nitrogen-doped graphene: A density functional theory study. *J. Catal.* **2011**, *282*, 183−190.
(34) Zhang, L. P.; Niu, J. B.; Dai, L.; Xia, Z. H. Effect of Microstructure of Nitrogen-Doped Graphene on Oxygen Reduction Activity in Fuel Cells. *Langmuir* **2012**, *28*, 7542−7550.
(35) Das, A.; Pisana, S.; Chakraborty, B.; Piscanec, S.; Saha, S. K.; Waghmare, U. V.; Novoselov, K. S.; Krishnamurthy, H. R.; Geim, A. K.; Ferrari, A. C.; Sood, A. K. Monitoring dopants by Raman scattering in an electrochemically top-gated graphene transistor. *Nat. Nanotechnol.* **2008**, *3*, 210−215.
(36) Casiraghi, C. Probing disorder and charged impurities in graphene by Raman spectroscopy. *Phys. Status Solidi R* **2009**, *3*, 175−177.
(37) Heydrich, S.; Hirmer, M.; Preis, C.; Korn, T.; Eroms, J.; Weiss, D.; Schuller, C. Scanning Raman spectroscopy of graphene antidot lattices: Evidence for systematic p-type doping. *Appl. Phys. Lett.* **2010**, *97*, 043113.
(38) Lee, J.; Novoselov, K. S.; Shin, H. S. Interaction between Metal and Graphene: Dependence on the Layer Number of Graphene. *ACS Nano* **2011**, *5*, 608−612.
(39) Wang, W. X.; Liang, S. H.; Yu, T.; Li, D. H.; Li, Y. B.; Han, X. F. The study of interaction between graphene and metals by Raman spectroscopy. *J. Appl. Phys.* **2011**, *109*, 07c501.
(40) Ryu, S.; Liu, L.; Berciaud, S.; Yu, Y. J.; Liu, H. T.; Kim, P.; Flynn, G. W.; Brus, L. E. Atmospheric Oxygen Binding and Hole Doping in Deformed Graphene on a SiO_2 Substrate. *Nano Lett.* **2010**, *10*, 4944−4951.
(41) Iqbal, M. W.; Singh, A. K.; Iqbal, M. Z.; Eom, J. Raman fingerprint of doping due to metal adsorbates on graphene. *J. Phys.: Condens. Matter* **2012**, *24*, 3335301.